J Appl Electrochem (2008) 38:1375–1383
DOI 10.1007/s10800-008-9575-6

ORIGINAL PAPER

Incorporation of zirconia nanoparticles into coatings formed on aluminium by AC plasma electrolytic oxidation

E. Matykina · R. Arrabal · P. Skeldon · G. E. Thompson

Received: 1 December 2007 / Revised: 17 April 2008 / Accepted: 21 April 2008 / Published online: 29 April 2008

Abstract Composite ceramic coatings were formed on aluminium by AC plasma electrolytic oxidation (PEO) using $Na_6P_6O_{18}$ or $Na_2SiO_3 \cdot 5H_2O$/KOH electrolytes with monoclinic zirconia nanoparticles in suspension. The coatings grown in $Na_2SiO_3 \cdot 5H_2O$/KOH electrolyte revealed γ-Al_2O_3 and amorphous phase; α-Al_2O_3 and $AlPO_4$ were additionally produced with the $Na_6P_6O_{18}$ electrolyte. Higher temperature zirconia phases, possibly tetragonal and orthorhombic, in addition to the monoclinic phase, were indicative of elevated temperatures at sites of microdischarges. Further, local melting resulted in zirconium-rich dendrites in the coating formed in silicate electrolyte. Zirconium was mainly located in the relatively compact, outer layer of the coating, constituting ~70–90% of the coating thickness. Nanoparticles appeared to be incorporated at the coating surface and following transport to the interface regions between the inner and outer layers along short-circuit paths through the outer coating.

Keywords Aluminium · Zirconia · Coatings · Plasma electrolytic oxidation

1 Introduction

Plasma electrolytic oxidation (PEO) can be employed for the production of hard coatings on aluminium alloys. The coatings are formed under DC or AC conditions above the dielectric breakdown voltage in a range of electrolytes. Microdischarges, with typical lifetimes up to the order 100 ms, are associated with temperature rises in the coating that can result in high-temperature phases, such as α-Al_2O_3, with high hardness. During PEO at constant current, the thickness of the coating increases approximately linearly with time, with typical coatings being of the order 10 μm thick. The coatings may contain cavities and channels of various sizes, with pores at the coating surface. The possibility of contributions from plasma-chemical, thermal and anodic oxidation processes leaves considerable uncertainty about the precise mechanism of coating formation. The present experiments introduce nanoparticles into the coating to probe transport processes and local temperatures.

Anodizing and plasma electrolytic electrophoresis have been used to fabricate composite ceramic coatings since at least the late 1970s [1, 2]. Suspensions of Al_2O_3 [1, 3, 4], SiO_2 [1] and SiC [5] have been employed to produce coatings with enhanced thermomechanical properties, reduced surface porosity and increased wear-resistance. An increased coating strength has been shown for PEO coatings formed in electrolytes with Al_2O_3, TiO_2, Cr_2O_3, ZrO_2, TiC, B_4C, BN particles [6]. Alumina films containing ~16 wt.% iron have been produced by PEO in an electrolyte containing iron particles [7, 8]. Further, α-Al_2O_3 colloidal particles have been suggested to penetrate the microplasma discharge zone to form coating material [4]. In the present work, zirconia particles are used to investigate the coating formation. The particular conditions employed for PEO were derived from trials to produce coatings with significant incorporation of zirconia. Such conditions can be of a significant interest for surface modification to produce zirconia toughened alumina (ZTA). ZTA has attracted interest and extensive research due to a combination of high fracture toughness and wear

E. Matykina (✉) · R. Arrabal · P. Skeldon · G. E. Thompson
Corrosion and Protection Centre, School of Materials,
The University of Manchester, P.O. Box 88,
Manchester M60 1QD, UK
e-mail: E.Matykina@manchester.ac.uk

and corrosion resistance. It finds applications in cutting tools [9–11], implants and dentistry [12, 13].

2 Experimental

2.1 PEO treatment

Specimens of 99.99% aluminium sheet were embedded in resin, with electrical connection provided through a shielded copper wire. The exposed surface, of area 1 cm^2, was degreased in ethanol, rinsed in deionized water and dried in warm air. The electrolytes, comprising either 50 g l^{-1} $Na_6P_6O_{18}$ (pH 9.0) or 30 g l^{-1} $Na_2SiO_3 \cdot 5H_2O$/2.8 g l^{-1} KOH (pH 12.5), were prepared from deionized water and high-purity chemicals. Additions of 10 g l^{-1} of monoclinic zirconia particles, of size 150–300 nm, were made as required. The electrolyte compositions were selected such as to provide sustainable sparking in AC regime and reasonably high coating growth rate of ~0.75–1 μm min^{-1}. AC PEO treatment was carried out at 10 A dm^{-2} (rms) for 2400 s at 50 Hz with a sinusoidal waveform. The coatings were formed in a 1 l double-walled glass cell through which a cooled water/glycol mixture was pumped in order to keep the electrolyte temperature close to 293 K. The electrolyte was stirred continuously during the treatment. A sheet of type 304 stainless steel, of size 7.5 × 15 cm, was used as the cathode. Voltage responses were recorded electronically, with a sampling time of 20 ms, employing an SCXI data acquisition system (National Instruments) with data analysis by Igor Pro (Wavemetrics). After coating, specimens were rinsed with deionized water and dried in warm air.

2.2 Specimen examination

PEO treated specimens were examined by scanning electron microscopy (SEM) and field emission gun SEM (FEG-SEM), using Amray 1810 and Philips XL30 instruments respectively, both equipped with EDX analysis facilities. Cross-sections were ground through successive grades of SiC paper, followed by finishing to 1 μm diamond. Phase composition was investigated by X-ray diffraction (XRD), using a Philips ΧPert-MPD (PW 3040) instrument with a step size 0.005° and a scan range from 5 to 85° (in 2θ). An electron-transparent section, nominally 100 nm thick, of a specimen treated in silicate electrolyte, with zirconia addition, was examined by high-resolution field emission gun transmission electron microscopy (FEG-TEM), using a TECNAI F30 G2 instrument, operated at 300 kV, with a Gatan imaging filter (GIF2001). The section was fabricated using a FEI Nova Lab Dual Beam focused ion beam facility.

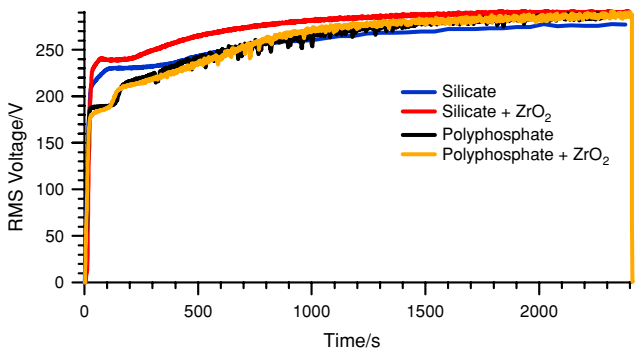

Fig. 1 Voltage-times responses for PEO of aluminium at 10 A dm^{-2} in $Na_6P_6O_{18}$ and $Na_2SiO_3 \cdot 5H_2O$/KOH electrolytes with and without addition of 10 g l^{-1} zirconia particles

3 Results

3.1 Voltage-time responses

The voltage-time responses revealed relatively rapid voltage rises to ~170 and 220 V in $Na_6P_6O_{16}$ and $Na_2SiO_3 \cdot 5H_2O$/KOH electrolytes respectively (Fig. 1). For both electrolytes, a short plateau preceded the relatively slow voltage increase to the final voltages of ~280–285 V. Visible sparking commenced at ~175 and 210 V for the $Na_6P_6O_{16}$ and $Na_2SiO_3 \cdot 5H_2O$/KOH electrolytes respectively. Gas evolution accompanied sparking. The addition of zirconia to the electrolytes had minor influence on the responses.

3.2 $Na_6P_6O_{18}$ electrolyte

Figure 2a shows a scanning electron micrograph of a plan view of the coating formed in zirconia-free $Na_6P_6O_{18}$ electrolyte, with a surface morphology typical of PEO. In cross-section, the coating is relatively porous, with micron- and sub-micron-sized pores (Fig. 2b). The coating thickness is in the range 20–30 μm; with the outer 10–20% of the coating appearing to be more compact. EDX mapping indicated aluminium and oxygen as primary constituents of the coating, with relatively low concentrations of phosphorus in most regions. Point analyses indicated atomic ratios of P:Al of 0.10, 0.02 and 0.36 at locations in the inner, middle and outer regions of the coating respectively, with a ratio of 0.17 from an area analysis of the coating surface of Fig. 2a (Table 1).

Figure 3a reveals the plan view of the coating formed in the presence of zirconia. The coating surface is distinguished from that of the previous specimen by the presence of numerous nodular features, with size from ~100 nm to ~20 μm. In cross-section, the coating is of variable thickness in the range 20–60 μm and is more compact than that formed in the absence of zirconia (Fig. 3b). Nodules projecting from the coating surface are in the size range of

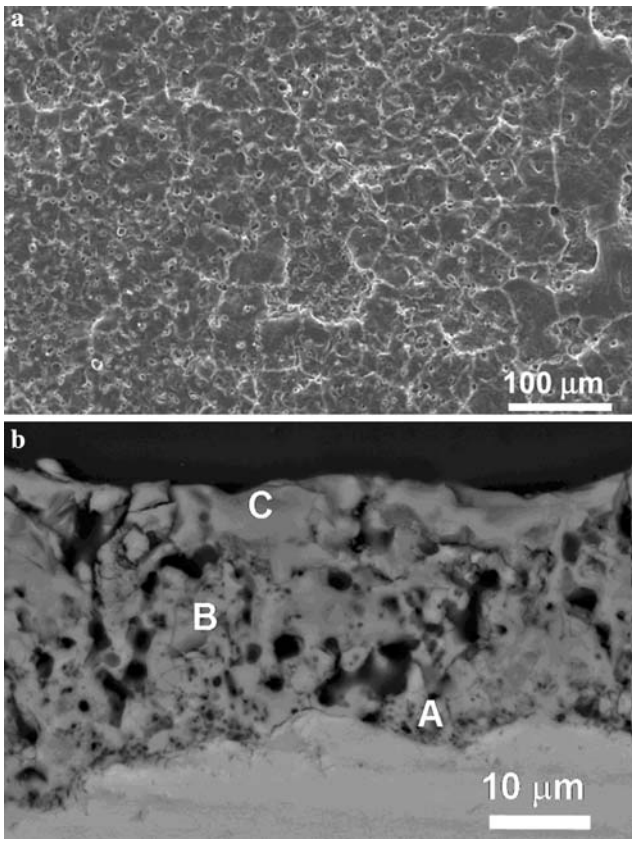

Fig. 2 Scanning electron micrographs of the coating formed on aluminium for 2400 s at 10 A dm^{-2} in $Na_6P_6O_{18}$ electrolyte. (**a**) Plan view (secondary electrons). (**b**) Cross-section (backscattered electrons)

the particle-like features observed in the plan view. The relatively light regions of the coating in the backscattered electron image contain increased amounts of zirconium relative to adjacent material, which was confirmed by EDX mapping. The inner 10–20% of the coating was of relatively dark appearance, with a high population density of fine pores, whereas the overlying outer layer consisted of compact material containing occasional large cavities. This inner region contained relatively little zirconium. Figure 3c shows a channel through the coating filled with material of high zirconium content. At the base of the channel, the zirconium appears to mix non-uniformly with the inner porous material. A thin band of material was present at the coating surface, which appeared to entrain zirconia particles. EDX point analyses were not carried out due to the proximity of peaks for zirconium and phosphorus. Occasional relatively large agglomerations of zirconia particles are incorporated into the outer coating regions. The most porous part of the inner coating was located near the aluminium/coating interface. A barrier-like region of coating, of thickness $\sim$500 nm, is present next to the interface.

Close examination of the outer coating layer disclosed a complex microstructure, which did not occur in the coating formed in zirconia-free electrolyte (Fig. 4). Relatively light features, indicative of increased zirconium content, ranged in size from $\sim$100 nm to several microns. These included zirconium-rich dendrites, which were distributed non-uniformly through the coating, with zones of coating material differing with respect to the dendrite size. XRD revealed the presence of $AlPO_4$, α-Al_2O_3 and γ-Al_2O_3 in coatings formed in zirconia-free and zirconia-containing electrolytes (Fig. 5). Broad peaks were present at $\sim$ 45° due to amorphous material. For the zirconium-containing electrolyte, strong peaks were also found for monoclinic zirconia and for zirconia in tetragonal or, possibly, orthorhombic form, which produce peaks at similar angles. Due to a very small difference of about $\sim$0.1–.04 2θ degrees between characteristic peaks of t-ZrO_2 and o-ZrO_2 and similar peak intensities it was not possible to separate these compounds accurately.

Table 1 Area and point EDX analysis (at.%) of coatings

Coating			Al	O	Si	P	Zr	Zr:Al	Si:Al	P:Al
Phosphate	Area		27.8	67.4	–	4.8	–	–	–	0.17
	Local	A-Inner	23.0	74.7	–	2.3	–	–	–	0.10
		B-Intermediate	25.6	73.9	–	0.5	–	–	–	0.02
		C-Outer	16.4	77.7	–	5.9	–	–	–	0.36
Silicate	Area		2.5	77.0	20.5	–	–	–	8.2	–
	Local	A-Inner	34.1	65.1	0.8	–	–	–	0.02	–
		B-Intermediate	26.0	68.7	5.3	–	–	–	0.20	–
		C-Outer	11.0	71.8	17.2	–	–	–	1.56	–
Silicate + ZrO_2	Area		4.1	58.5	23.7	–	13.7	3.34	5.78	–
	Local	A-Inner	13.1	70.6	7.5	–	8.8	0.08	0.12	–
		B-Intermediate	27.7	66.8	3.4	–	2.1	0.67	0.58	–
		C-Outer	0.5	60.9	1.6	–	37.1	74.2	3.20	–

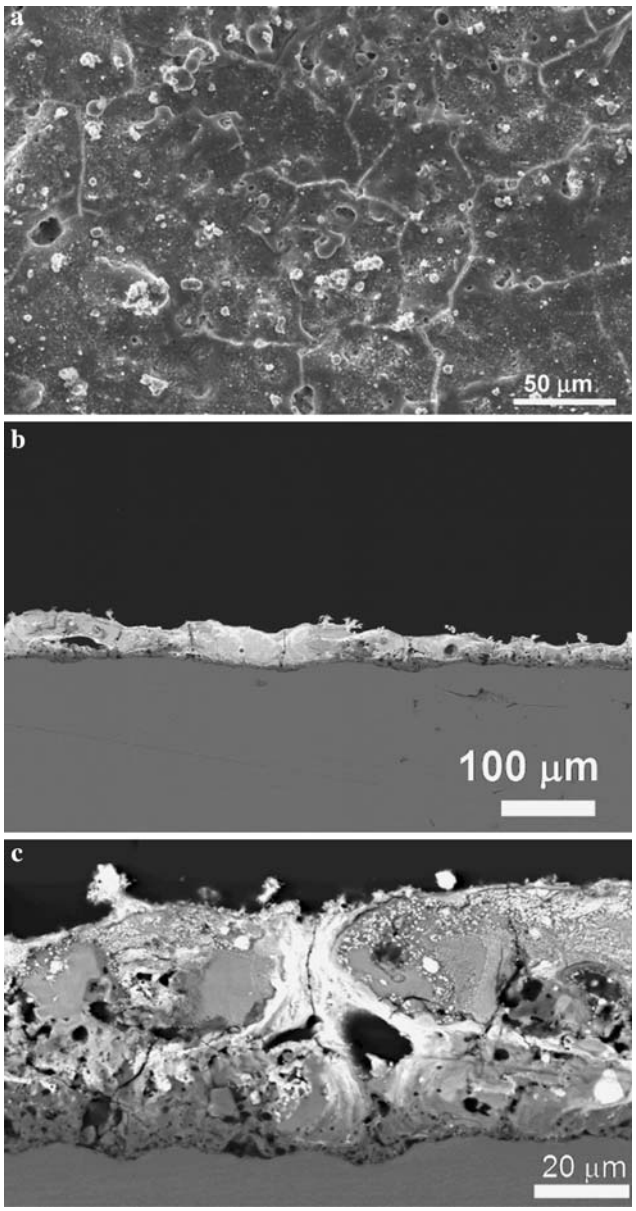

Fig. 3 Scanning electron micrographs of the coating formed on aluminium for 2400 s at 10 A dm^{-2} in $Na_6P_6O_{18}$ electrolyte with addition of 10 g l^{-1} zirconia particles. (**a**) Plan view (secondary electrons). (**b**, **c**) Cross-sections (backscattered electrons)

3.3 $Na_2SiO_3 \cdot 5H_2O$/KOH

Figure 6a, b reveal the plan and cross-section views of the coating formed in the $Na_2SiO_3 \cdot 5H_2O$/KOH electrolyte, with a thickness ranging from ~15–30 μm. The inner ~10–30% of the coating is more finely porous than the overlying region. EDX point analyses indicated increased silicon at the coating surface, with atomic ratios of Si:Al of 0.02 in the inner coating, 0.20 in the more compact material of the outer coating and 1.56 near the coating surface (Table 1).

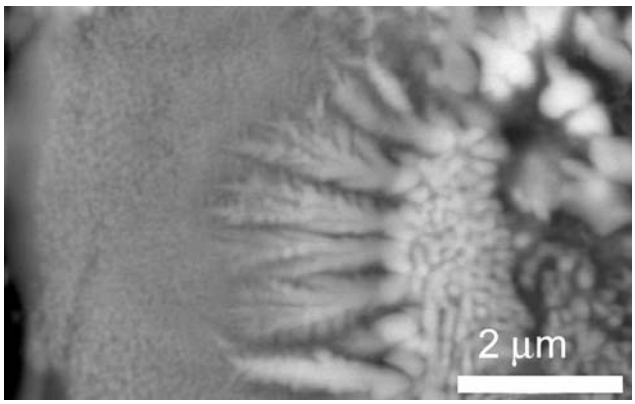

Fig. 4 Scanning electron micrograph (backscattered electrons) of the coatings formed on aluminium for 2400 s at 10 A dm^{-2} in $Na_6P_6O_{18}$ electrolyte with addition of 10 g l^{-1} zirconia particles

In contrast to the relatively smooth coating surface of Fig. 6a, the coating developed in the presence of zirconia was decorated by nodular features of size ranging from ~100 nm to ~10 μm (Fig. 7a), similarly to the coating formed in $Na_6P_6O_{18}$ electrolyte containing zirconia. The coating thickness varied from 15–65 μm, as shown in Fig. 7b. The inner ~10–30% of the coating was more finely porous than the outer region, and was darker in appearance in backscattered electron image due to a reduced amount of zirconium (Fig. 7c). Zirconium-rich particles frequently appeared to decorate the peripheries of larger pores in the outer coating regions (Fig. 7c). EDX point analyses revealed atomic ratios of Si:Al of 0.12 and 0.58 in the inner more porous coating and in the overlying more compact region respectively (Table 1). Area analyses of the coating surface revealed a high silicon enrichment, with an Si:Al ratio of 5.78.

The zirconium-containing coating disclosed features similar to those observed for the $Na_6P_6O_{18}$ electrolyte with addition of zirconia, with zirconium-rich dendrites in the outer coating layer (Fig. 8a). Figure 8a also shows an agglomeration of nanoparticles that has been incorporated in the coating. The inner coating near the aluminium contained relatively little zirconium, with greatest porosity being located just above the barrier layer at the aluminium/coating interface (Fig. 8b). EDX mapping indicated the presence of silicon species in most regions of the coating. However, less silicon was present in the inner, more porous coating, which also contained reduced amounts of zirconium. Silicon appeared to be enriched at the coating surface, including regions of projecting material. EDX point analyses revealed atomic ratios of Zr:Al of ~0.08 and 0.67 in the inner layer and the immediately overlying, more compact region respectively. Agglomerations of zirconia particles were most prevalent toward the coating surface, suggesting that they are incorporated into the

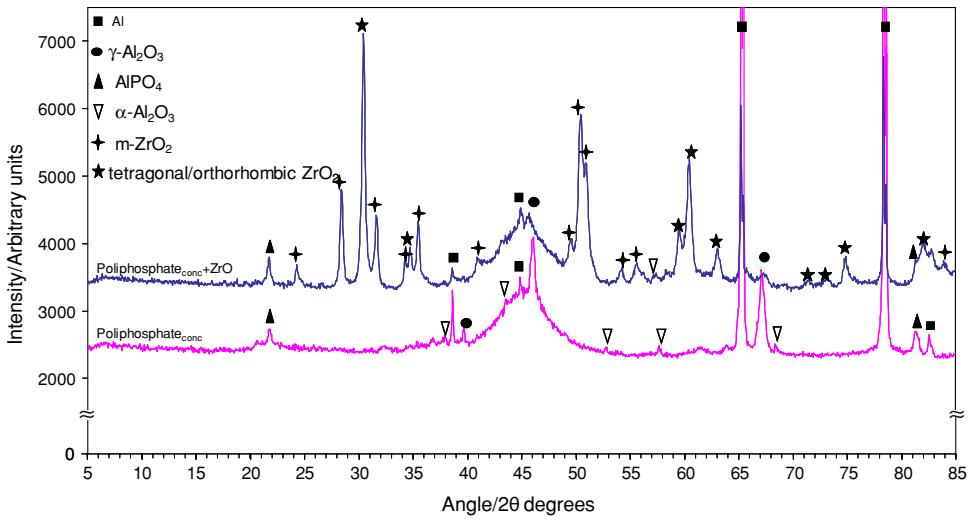

Fig. 5 XRD pattern for aluminium following PEO treatment for 2400 s at 10 A dm^{-2} in $Na_6P_6O_{18}$ electrolyte with and without addition of 10 g l^{-1} zirconia particles

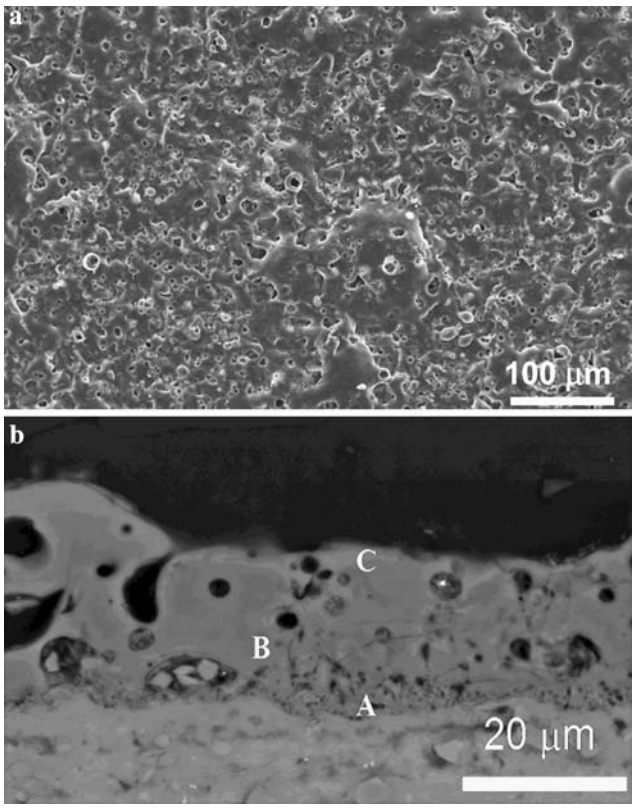

Fig. 6 Scanning electron micrographs of the coating formed on aluminium for 2400 s at 10 A dm^{-2} in $Na_2SiO_3 \cdot 5H_2O$/KOH electrolyte. (**a**) Plan view (secondary electrons). (**b**) Cross-section (backscattered electrons)

coating at the coating surface. EDX point analyses of the agglomerations revealed a Al:Zr ratio of ~0.01.

Results of XRD revealed strong peaks for mullite and lesser peaks for γ-Al_2O_3 in the coating formed in the zirconia-free electrolyte (Fig. 9). In contrast, no peaks for mullite were found for the coating with incorporated zirconium species, for which weak peaks for γ-Al_2O_3. A broad peak at ~45° indicated the presence of amorphous material of short-range for the coating formed in the absence of zirconia. The peak was much reduced for the coating containing zirconium species. Low broad peaks were also present for both coatings at ~20–30° indicative of amorphous material of increased mean scattering length. Monoclinic zirconia was present in the coatings formed in electrolyte containing zirconia particles. In addition peaks were also identified for tetragonal or orthorhombic forms.

Transmission electron micrographs of the coating formed in electrolyte containing zirconia revealed relatively extensive regions of amorphous coating material with incorporated zirconia particles (Fig. 10a). Monoclinic zirconia was identified in a particle located near the barrier layer at the base of the coating, with the particles size being within the range of the particles added to the electrolyte (Fig. 10b). In the middle region of the coating, particles were disclosed with modified morphologies, with electron diffraction indicating a combination of monoclinic and orthorhombic zirconia (Fig. 10c).

4 Discussion

The findings of the study demonstrate the incorporation of zirconia particles into coatings formed on aluminium by PEO under AC conditions. The zirconium is present in the coating as discrete particles, similar in size to those of the suspension, as occasional agglomerations of particles, as zirconium-rich regions in channels, and in the main coating material, where zirconium-containing dendrites are evident with a range of size, including both smaller and larger than the size of the original particles. The formation of the dendrites indicates melting of the coating material at microdischarge sites and the subsequent precipitation of

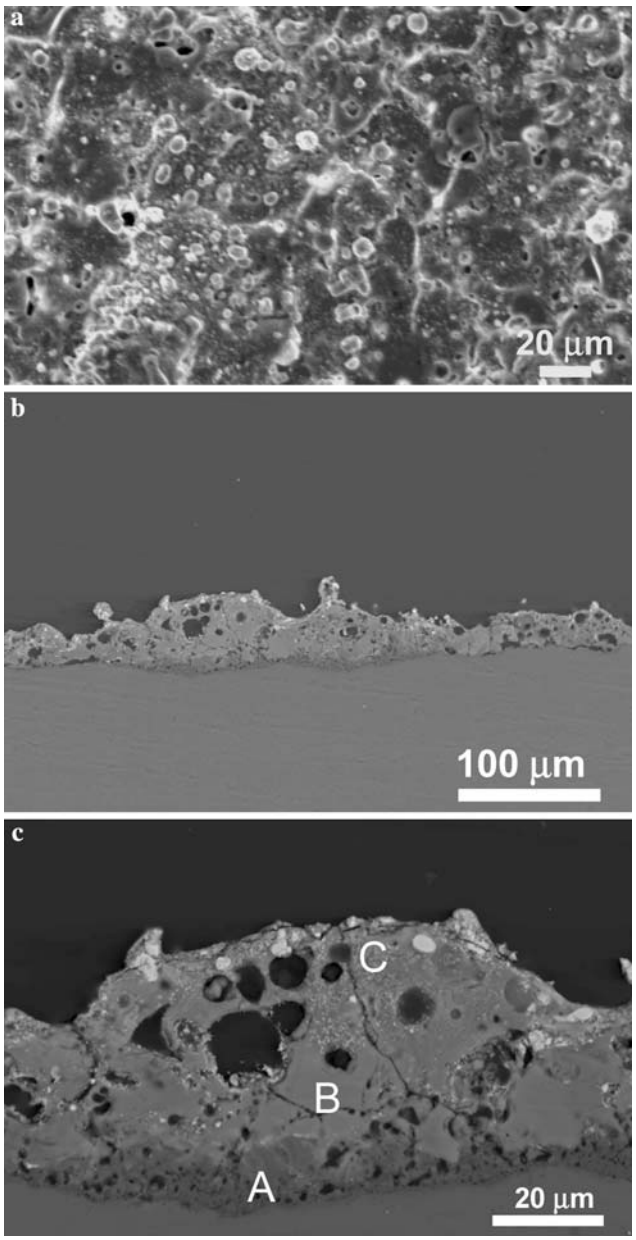

Fig. 7 Scanning electron micrographs of the coating formed on aluminium for 2400 s at 10 A dm^{-2} in $Na_2SiO_3 \cdot 5H_2O$/KOH electrolyte with addition of 10 g l^{-1} zirconia particles. (**a**, **b**) Plan views (secondary electrons, (**b**) with tilt). (**c**, **d**) Cross-sections (backscattered electrons)

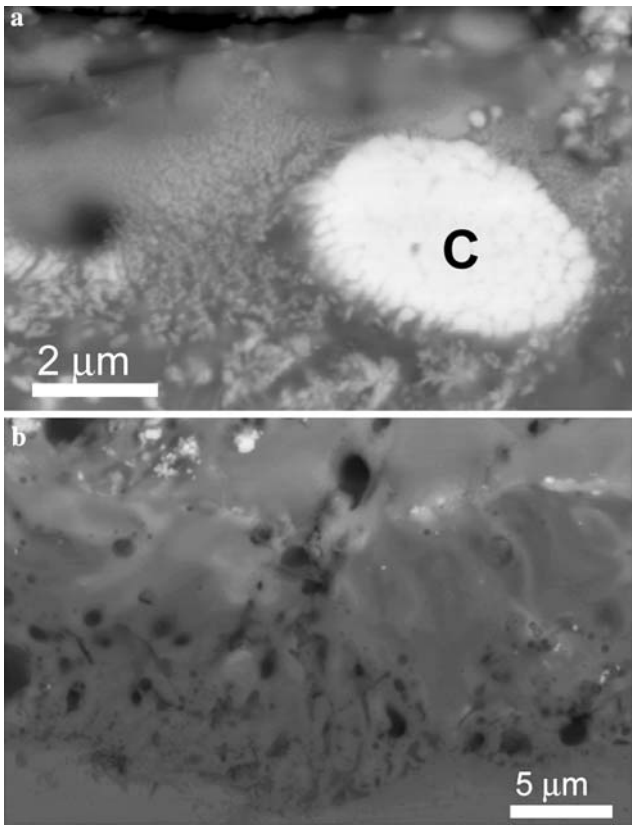

Fig. 8 Scanning electron micrographs (backscattered electrons) of the coating formed on aluminium for 2400 s at 10 A dm^{-2} in $Na_2SiO_3 \cdot 5H_2O$/KOH electrolyte with addition of 10 g l^{-1} zirconia particles. (**a**) Outer coating. (**b**) Inner coating

zirconium-rich phase during cooling and subsequent solidification. Heat is conducted away from the microdischarge site through the coating and through the aluminium substrate, with the relatively low thermal conductivity of the coating [14] assisting the rise in temperature. The elevated temperature results in the formation of tetragonal or orthorhombic zirconia, or possibly both structures. The orthorhombic structure is known to form from tetragonal zirconia under high pressures [15, 16] or fast densification of material and is formed for instance in magnesia- or yttria-stabilised zirconia as an intermediate phase of the transformation of the tetragonal phase to monoclinic phase [17, 18]. The monoclinic zirconia in the coating may be either untransformed zirconia particles of the suspension or the product of transformation of the higher temperature structures on cooling of the coating. Monoclinic zirconia transforms to tetragonal zirconia above ~1240 °C, with the reverse transformation taking place at ~1170 °C [19]. However, the absence of the cubic form of zirconia suggests that temperatures of tetragonal-to-cubic transformation 2370 °C have not been reached.

The distribution of zirconium in the coatings suggests that particles can be incorporated at the coating surface. They can also be transported along short-circuit paths to the inner coating regions. At the high local temperatures of the microdischarge, evaporation of the electrolyte may concentrate, transform and deposit electrolyte constituents at the coating surface. The particle transport in the electrolyte to the coating may also be assisted by electrophoresis. The molten coating phase, containing aluminium, phosphorus, silicon and possibly sodium and

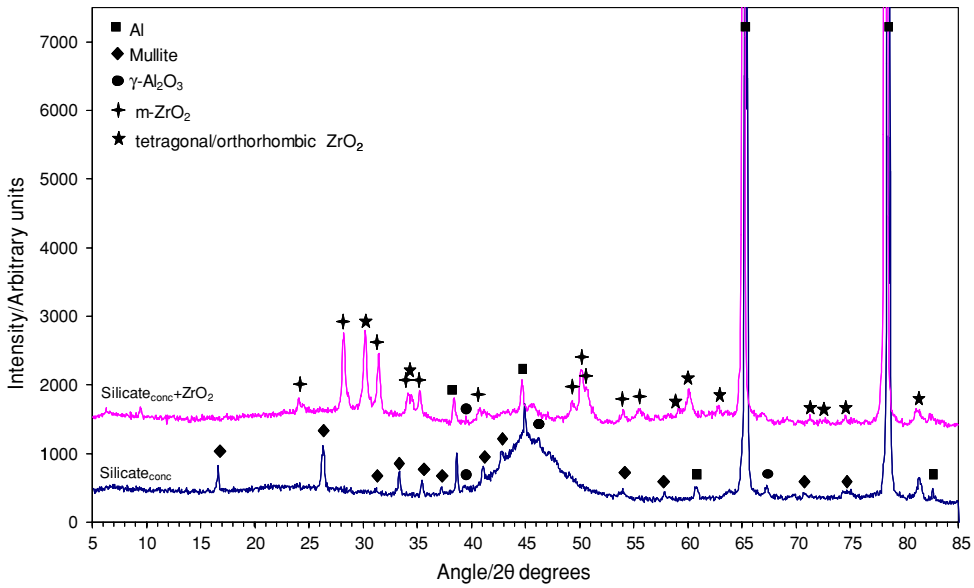

Fig. 9 XRD pattern for aluminium following PEO treatment for 2400 s at 10 A dm^{-2} in $Na_2SiO_3 \cdot 5H_2O$/KOH electrolyte with and without addition of 10 g l^{-1} zirconia particles

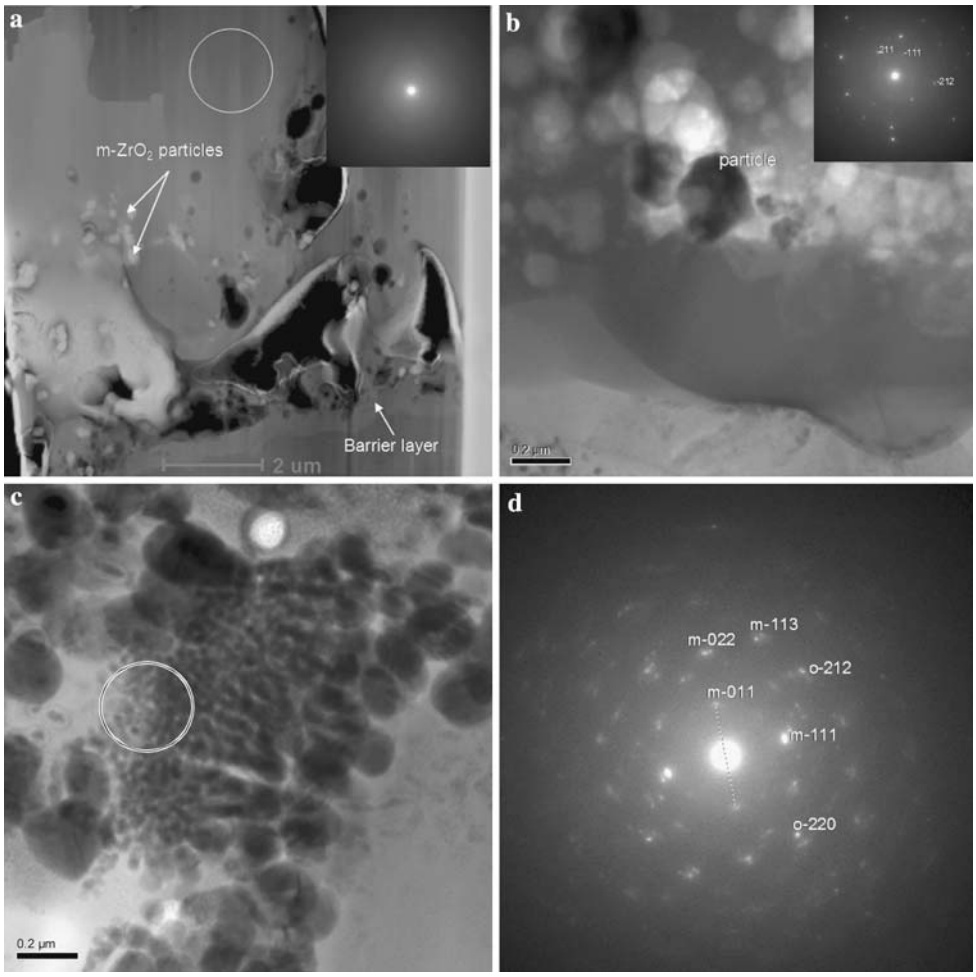

Fig. 10 Transmission electron micrographs and electron diffraction patterns of the coating formed on aluminium for 2400 s at 10 A dm^{-2} in $Na_2SiO_3 \cdot 5H_2O$/KOH electrolyte with addition of 10 g l^{-1} zirconia particles. (**a**) Low magnification image, showing mainly amorphous coating material with incorporated zirconia particles. (**b**) Particle of monoclinic zirconia near barrier layer at aluminium/coating interface. (**c**) Transformed zirconia particles, with electron diffraction indicating monoclinic and orthorhombic zirconia

potassium species, dissolves the zirconia, which later precipitates on termination of the microdischarge and cooling of the coating. Within the melted region, zirconium may be transported by diffusion, migration and by convection. Due to the potential presence of a range of constituents, the solidification temperature of the coating is uncertain.

Further, the size and number of zirconia dendrites depends upon factors such as the local concentrations of zirconium in the melted region, temperature gradients in the solidification zone and the rate of solidification. The distribution of zirconium will also be affected by repetition of microdischarges at and near a particular site. The incorporation of zirconium species into the coatings did not alter the types of crystalline phase in the coatings formed in $Na_6P_6O_{18}$ electrolyte, although they may be changed in relative amounts. In contrast, the zirconium species strongly suppressed the formation of mullite in the coatings formed in $Na_2SiO_3 \cdot 5H_2O$/KOH electrolyte. The absence of Al–Zr–O crystalline phase in the coatings is consistent with the Al_2O_3–ZrO_2 phase diagram, which reveals a eutectic temperature of 1840 ± 10 °C at a composition of 40% ZrO_2 with formation of Al_2O_3 and ZrO_2 with relatively low solubility of zirconia and alumina respectively [20]. The formation of zirconium-rich dendrites suggests a local melt phase exceeding the eutectic composition for zirconia.

The inner 10–30% of the coatings contained significantly less zirconium than the outer coating. The inner region also appeared more finely porous, with porosity increasing toward the aluminium substrate. The porosity of the inner coating is possibly related to the gas generation that accompanies coating growth, including oxygen and hydrogen during anodic and cathodic cycles respectively. The numerous, approximately spherical pores in the inner coating suggest that the inner material can flow to accommodate pore development. The difference in composition of the inner and outer coating regions is possibly related to the short-circuit transport of electrolyte components through the outer coating, which has been identified previously [21–24]. Thus, the physical and thermal properties of the inner coating material may be significantly different from those of the outer coating. The aluminium species in the outer coating must be transported across the inner coating region. The outer coating possibly contains material of higher melting point, such that components of the inner coating that are transported to the inner coating/outer coating interface segregate as higher melting point phase.

A barrier layer of thickness ~500 nm was present at the aluminium/coating interface. The thickness of the barrier layer is consistent with a formation ratio of ~1 nm V^{-1} that is typical of anodic alumina formation at ambient temperatures. The barrier layer contains aluminium that is oxidized at the final stages of the microdischarge when the local temperature is probably decreasing. Transmission electron microscopy disclosed amorphous alumina in the barrier region. The similarity of the barrier layer thickness to that expected for conventional anodizing at the final PEO voltage suggests that the electrolyte has ready access to the barrier region, presumably due to the channels, cavities, pores and cracks in the coating.

5 Conclusions

1. Monoclinic zirconia nanoparticles can be incorporated into PEO coatings under AC conditions on aluminium in polyphosphate and silicate electrolytes. During coating growth higher temperature forms of zirconia are developed due to the elevated temperatures at sites of microdischarges, in the range of 1840–2370 °C.
2. The main coatings comprise an outer more compact layer and inner finely porous layer; a relatively thin barrier layer is present at the aluminium/coating interface. The incorporation of zirconia significantly alters the microstructure of the coatings, with zirconium-rich dendrites forming in the outer coating regions.
3. Nanoparticles can be transported along short-circuit paths though the outer coating to the interface with the coating material of the inner layer. Additionally, individual and agglomerations of nanoparticles appear to be incorporated at the coating surface.
4. The presence of zirconia suppresses the formation of mullite in coatings produced in silicate electrolyte. In contrast, crystalline aluminium phosphate occurs in coatings formed in polyphosphate electrolyte irrespective of the presence of zirconia.
5. PEO is a promising surface treatment technique for fabrication of zirconia-toughened alumina, which allows stabilisation of zirconium in tetragonal and orthorhombic forms.

Acknowledgement The authors are grateful to the Engineering and Physical Sciences Research Council (UK) for support of this work.

References

1. Saifullin RS (1992) In: Physical chemistry of inorganic polymeric and composite materials. Ellis Horwood, New York, London
2. Saifullin RS (1977) Composite coatings and materials. Khimia, Moscow
3. Bakovets VV, Polyakov OV, Dolgovesova IP (1991) Plasma electrolytic anode treatment of metals. Nauka, Novosibirsk
4. Khokhryakov Y, Butyagin P, Mamaev A (2005) J Mater Sci 40:3007–3008
5. Wang YK, Sheng L, Xiong RZ, Li BS (1999) Surf Eng 15: 109–111
6. Malyshev VN, Zorin KM (2007) Appl Surf Sci 254:1511–1516
7. Jin F, Tong H, Li J, Shen L, Chu PK (2006) Surf Coat Technol 201:292–295
8. Jin F, Chu PK, Tong H, Zhao J (2006) Appl Surf Sci 253: 863–868
9. Novak S, Kalin M, Lukas P, Anne G, Vleugels J, Van Der Biest O (2007) J Europ Ceram Soc 27:151–156

10. Sarkar D, Adak S, Chu MC, Cho SJ, Mitra NK (2007) Ceram Int 33:255–261
11. Magnani G, Brillante A (2005) J Europ Ceram Soc 25:3383–3392
12. Pierri J, Roslindo EB, Tomasi R, Agnolon Pallone EMJ, Rigo ECS (2006) J Non-Cryst Solids 352:5279–5283
13. Gutknecht D, Chevalier J, Garnier V, Fantozzi G (2007) J Europ Ceram Soc 27:1547–1552
14. Curran JA, Clyne TW (2005) Surf Coat Technol 199:177–183
15. Kudoh Y, Takeda H, Arashi H (1986) Phys Chem Minerals 13:233
16. Haines J, Leger JM, Atouf A (1995) J Am Ceram Soc 78:445
17. Guinebretihe R, Oudjedi Z, Dauger A (1996) Scripta Materialia 34:1039–1044
18. Liang B, Ding C, Liao H, Coddet C (2006) Surf Coat Technol 200:4549–4556
19. Ryshkewitch E (1960) Oxide ceramics. Academic, New York
20. Jerebtsov DA, Mikhailov GG, Sverdina SV (2000) Ceram Int 26:821–823
21. Matykina E, Monfort F, Berkani A, Skeldon P, Thompson GE, Chapon P (2006) Phil Mag 86:49–66
22. Matykina E, Monfort F, Berkani A, Skeldon P, Thompson GE, Gough J (2007) J Electrochem Soc 154:C279–C285
23. Monfort F, Berkani A, Matykina E, Skeldon P, Thompson GE, Habazaki H, Shimizu K (2005) J Electrochem Soc 152: C382–C387
24. Monfort F, Matykina E, Berkani A, Skeldon P, Thompson GE, Habazaki H, Shimizu K (2007) Surf Coat Technol 201: 8671–8676